EFFECT OF SQUEEZE CASTING AND COMBINED ADDITION OF CALCIUM AND STRONTIUM ON MICROSTRUCTURE AND MECHANICAL PROPERTIES OF AZ91 MAGNESIUM ALLOY

Ankush S. Marodkar, Hitesh Patil and Hemant Borkar
Department of Metallurgy Engineering and Materials Science, Indian Institute of Technology Indore, Simrol, Indore, Madhya Pradesh 453552, India

Amit Behl
Hero MotoCorp Ltd., Neemrana 301705, India

https://doi.org/10.1007/s40962-022-00943-1

Abstract

In the present work, the effect of squeezing at 100 MPa during AZ91 Mg alloy casting has been studied, where the microstructure, texture, and mechanical properties of gravity die-cast (GC) and squeeze cast (SC) AZ91 alloy samples have been compared. Also, the effect of the combined addition of calcium (Ca) and strontium (Sr) on microstructure and mechanical properties of AZ91 alloy fabricated by SC has been investigated. The SC AZ91 alloy samples exhibited weaker texture than that of GC AZ91 alloy with a reduction in maximum texture intensity. The squeeze casting resulted in the refinement of the secondary phase (β-$Mg_{17}Al_{12}$) in the microstructure by reducing its segregation at the grain boundaries. The volume fraction of β-$Mg_{17}Al_{12}$ was more suppressed with Ca and Sr alloy addition due to the formation of new Al_2Ca and Al_4Sr intermetallics. The tensile properties of SC AZ91 samples were found to be better than that of GC AZ91 samples. Further improvements in mechanical properties were obtained after alloying with Ca and Sr, and the best combination of all tensile properties was obtained at (1% Ca + 0.9% Sr) addition. Higher Sr addition than 0.9% Sr degraded the strength as it induced brittleness in the material.

Keywords: *magnesium alloys, AZ91 alloy, squeeze casting, texture analysis, mechanical properties, grain refinement*

Introduction

In the past decade, magnesium (Mg) alloys have been proving to be a significant attraction for aerospace and automobile applications owing to their notable characteristics like excellent strength-to-weight ratio resulting in a considerable reduction in oil consumption and hence fewer emissions.[1–4] AZ91 alloy (Mg-Al system) is the extensively used cast alloy in the automotive industries, accounting for 90% of all Mg cast products.[5–7] AZ91 mainly consists of two phases, i.e., primary α-Mg matrix and secondary eutectic β-$Mg_{17}Al_{12}$ precipitates. The β-$Mg_{17}Al_{12}$ has a vital role in the dispersion hardening and casting of Mg-Al alloys.[8–10]

During gravity die casting (GC), the β-$Mg_{17}Al_{12}$ mainly precipitates at the grain boundaries (GBs). As these β-$Mg_{17}Al_{12}$ precipitates are brittle in nature, they act as crack nucleation sites when they undergo mechanical deformation. Hence, precipitation of bulky secondary β-$Mg_{17}Al_{12}$ phase at GB deteriorates the mechanical properties of AZ91.[11,12] This problem can be resolved with the squeeze casting process. The squeeze casting process breaks down the coarser precipitates of secondary β-$Mg_{17}Al_{12}$ and gives a uniform and refined network of β-phase. Hence, improved mechanical properties could be obtained.[12]

Although having these superior properties, AZ91 lacks in strength, has limited cold workability, toughness, and poor corrosion and wear resistance.[13–15] Hence, alloying is the mainly used method to enhance the strength of Mg-Al alloy through microstructural refinement.[16,17] With this, it has

Received: 28 August 2022 / Accepted: 25 November 2022 / Published online: 4 January 2023

been found that the alloying addition increases the nucleation sites during the solidification process by forming their thermally stable precipitates with Al and Mg mainly at the grain boundaries resulting in refined microstructure and secondary phases in Mg-Al alloy.[8] These thermally stable precipitates act as effective barriers against dislocation and grain boundary movement even at higher temperatures.[1,18] Hence, improved strength can be obtained after alloying additions to certain limits.

Several works of the literature are available for improvement in the strength of Mg-Al alloy with the rare-earth (RE) alloying process. RE elements are added to the Mg alloys to improve their fluidity and mechanical strength.[19–21] With the addition of RE elements, RE intermetallics, having a higher melting point, are formed, enhancing the corrosion resistance and thermal stability of Mg alloys. With these superior properties, REs can form a new combination of additives for the improvement of Mg alloy. But their industrial implementation is limited due to high cost and less availability. Whereas being less expensive and largely available, alkaline-earth metals, Ca and Sr form thermally stable second phases with Al at grain boundaries leading to effective restriction to grain boundary sliding and migration. Also, Ca and Sr have negligible solubility in Mg at elevated temperatures compared to REs.[22–25] The Mg-Al–Zn–Ca–RE alloy series was newly developed,[26,27] which is employed for automatic transmission housings systems in automobiles. Xue Feng et al.[28] stated that the limited Ca addition to the AZ91 cast alloy resulted in enhancement of yield strength and significant microstructure refinement. Some Ca content dissolved into β-$Mg_{17}Al_{12}$, strengthening the alloy at elevated temperatures and improving its thermostability. Similar results were obtained in the study by Yang Zhang et al.[29] in which 1 wt% Ca addition to AZ91 cast alloy exhibited a satisfactory combination of mechanical properties in squeeze casting, whereas more than 1 wt% Ca induced brittleness in the material. Also, the addition of Sr in Mg-Al-based alloys could be an economical replacement for the rare-earth metals (REs) to improve mechanical properties at ambient as well as elevated temperatures.[30] Yu Fan et al.[31] showed 10.3% and 55.3% improvement in the UTS and % elongation, respectively, with 2 wt% Sr addition to cast AZ91 alloy as Sr promotes secondary particle strengthening as well as acts as a secondary phase refiner. In contrast, P. Zhao et al.[32] showed the highest improvement in UTS (25%) and % elongation (62.5%) with 0.1 wt% Sr addition in Mg–5Al–*x*Sr cast alloys (x = 0, 0.02, 0.1, 0.4, 0.7, 1). One of the authors of this work, H. Borkar, has previously studied the grain refining effect of Sr level (0.3 to 2.1 wt%) on die-cast Mg-1%Mn alloy in which it was observed that the reduction in average grain size occurred with the increase in Sr level up to 0.7 wt% with grain size remaining constant with further increase in Sr level.[33] Hence, it can be concluded that there is high uncertainty in optimum Sr amount as an alloying addition to Mg-Al alloys, and there is further scope to study its effect and optimization.

There are limited works in the literature on squeeze casting of AZ91 alloy. The current work first focuses on the effect of squeeze casting on the microstructure, texture and mechanical properties of AZ91 alloy. Texture study on squeeze casting is a novel work, and very less literature is available for texture analysis after squeeze casting of Mg alloys. Furthermore, an attempt has been made to study the effect of the combined addition of Ca and Sr on microstructure and mechanical properties of squeeze cast AZ91 alloy. Accordingly, in this study, the correlation in the formation of new phases after alloy addition (Ca + Sr) and its effect on microstructural characteristics such as morphology and volume fraction of β-phase, average grain size and secondary dendrite arm spacing (SDAS) has been investigated. Subsequently, the effect of various levels of Ca + Sr addition in squeeze cast AZ91 on mechanical properties including microhardness and tensile properties has been analyzed.

Experimental Procedure

Casting of Alloys

The commercial AZ91 Mg alloy ingot and Mg-Ca master alloy (Mg–20 wt% Ca) and Mg-Sr master alloy (Mg–20 wt% Sr) were used to prepare squeeze cast AZ91-Ca-Sr (SC AZ91-Ca-Sr) alloy samples. Gravity die-cast AZ91 (GC AZ91) and squeeze cast AZ91 (SC AZ91) alloy samples were also cast for reference. The bottom pouring-type stir casting machine was used to produce squeeze cast alloy samples. In this setup, an electrical resistance furnace was used to melt the material, while pouring was done using a bottom pouring arrangement which further connected to the squeeze casting setup. The same machine can also prepare gravity die-cast samples. The step-wise procedure followed to obtain GC and SC alloys is shown in Figure 1, and the bottom pouring-type stir casting machine setup is given in Figure 2. After preheating of melting furnace at 700 °C, the required amount of AZ91 alloy was added to the melting crucible. The melt was held at this temperature for 60 min for complete melting. The measured quantities of Mg-Ca and Mg-Sr master alloys were added to the melt and the melt was allowed to stabilize for 10 mins with uniform stirring at 300 rpm. All procedures were carried out under protective argon (99.5 vol%) + SF_6 (0.5 vol%) atmosphere to avoid oxidation. At 700 °C, the molten metal was poured into a cylindrical cast-iron mold (for both GC and SC alloys) through the bottom pouring arrangement. Before pouring the melt, the mold was coated with a thin layer of graphite oil and preheated at 200 °C by using an external heater arrangement. To obtain squeeze cast rods with 40-mm diameter and 300-mm length, the

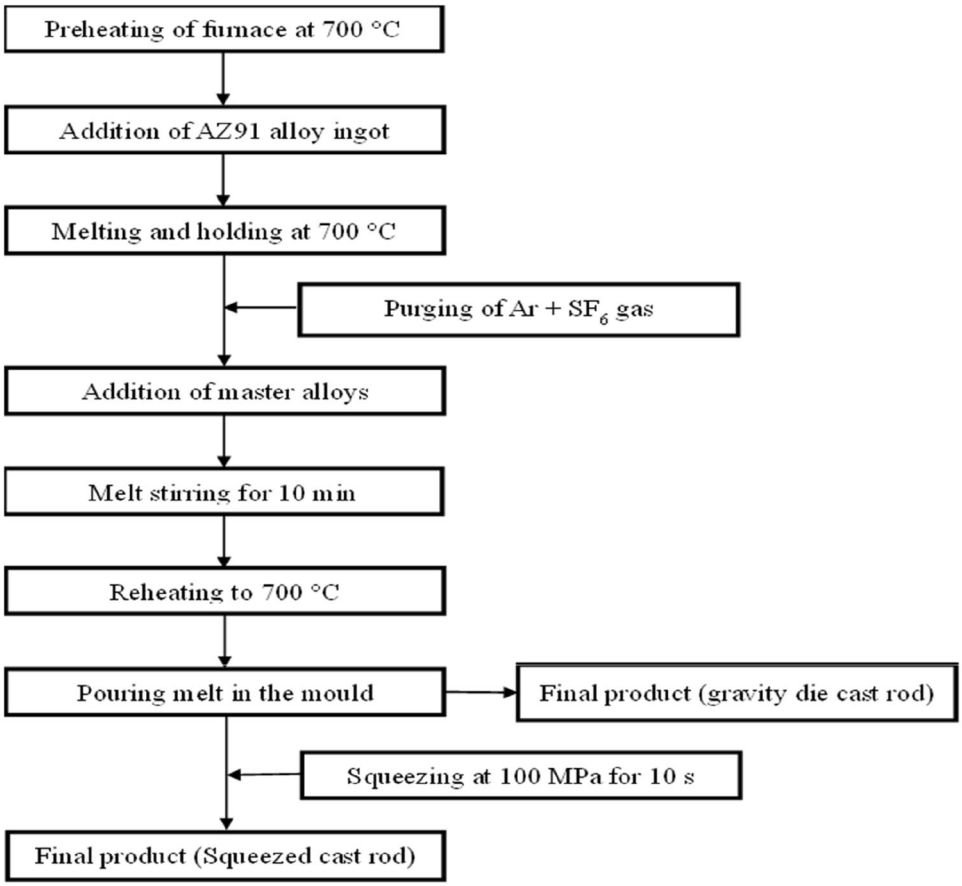

Figure 1. Flowchart showing the detailed steps followed for the fabrication of the AZ91 alloys.

squeezing process was done as soon as pouring was completed at 100 MPa for 30 s. The list of casting parameters is shown in Table 1. The various targeted and obtained combinations of Ca and Sr with AZ91 alloys and their respective alloy codes are shown in Table 2.

Characterization of Alloy Samples

The general metallographic technique was used for sample preparation for microscopic study of cast alloy samples. To reveal the microstructure, acetic picral solution (6 gm picric acid, 3 ml acetic acid, 100 ml ethanol, 10 ml DI water) was used to etch the samples after final polishing. The microstructure was analyzed using optical microscopy (OM, Zeiss axiovert a1 inverted microscope) and field emission scanning electron microscopy (FE-SEM, JEOL, JSM-7610 F plus). The micro-texture analysis and average grain size were measured using the electron backscattered diffraction (EBSD) technique. The data were obtained using FE-SEM (at 15 kV current and 15 kV voltage for 70° tilt sample) and analyzed with the Aztec HKL software. To prepare the samples for the EBSD scan, a final step of cloth polishing with 0.04-micron-sized colloidal silica for 30 min was used over the mirror-polished samples. The phases present in samples were detected by an X-ray diffractometer (XRD, PAN analytical X'Pert High Score) employing CuKα (λ=1.541Å) radiation. The X-ray scanning was carried out in the range (2θ) of 10°–90° with a step size of 0.04. The approximate percentage of volume fraction of second phases present and secondary dendrite arm spacing (SDAS) in the obtained alloys was calculated using ImageJ software using six different locations in the test samples. For sufficient accuracy, the SDAS was determined by measuring more than 50 dendrites arms for each specimen. Figure 3 shows the process used to measure SDAS (an optical image of A5 alloy is used). A set of lined-up cells was intersected by a straight line, and the number of cells was divided by the length of the line. Figure 4 illustrates the sample locations where the samples were extracted from each obtained cylindrical casting.

Microhardness and Tensile Testing

Vickers microhardness tests were performed using Micro-Vickers hardness tester (HM 112, Mitutoyo Co., Tokyo, Japan). Hardness testing was done at 300 g load and 15 s dwell time with six measurements for each sample, and average HV was plotted. Tensile testing was carried out by

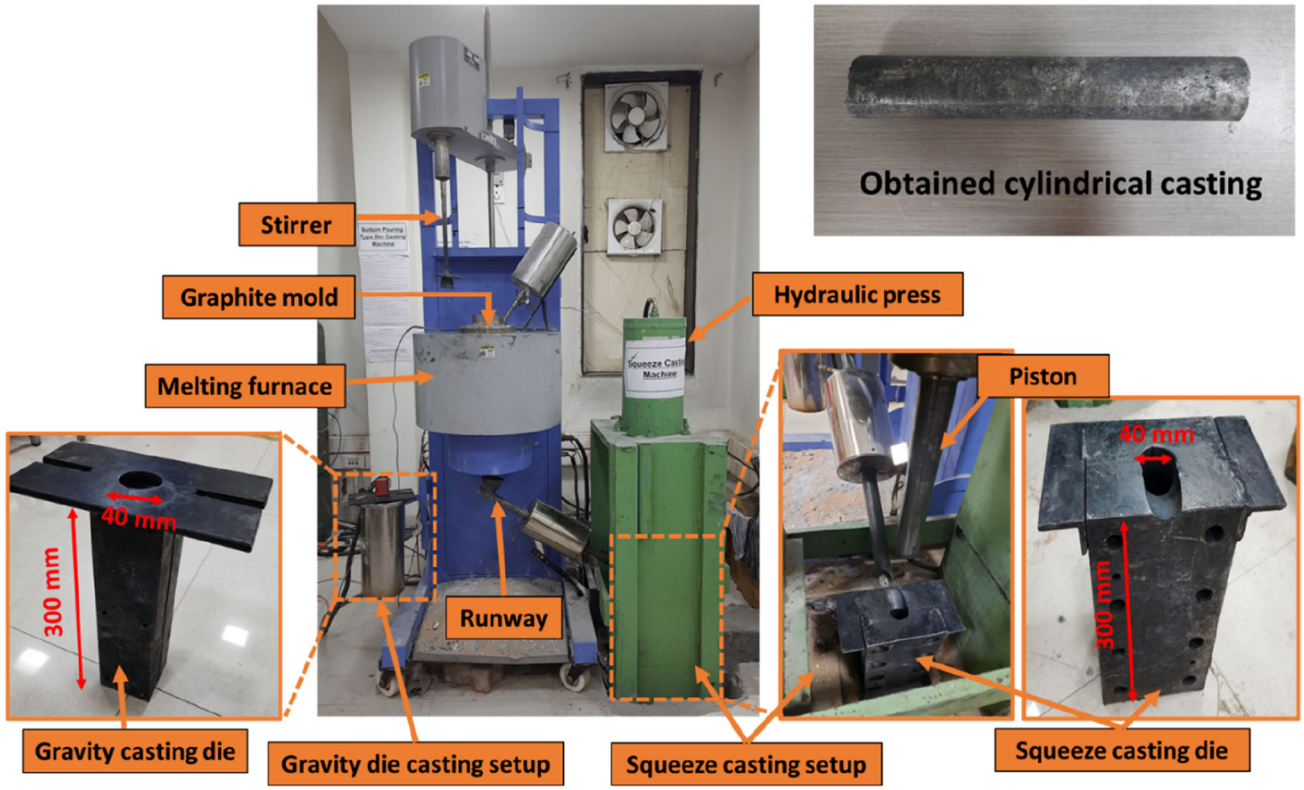

Figure 2. Bottom pouring-type stir casting machine setup.

Table 1. Gravity Die Casting and Squeeze Casting Parameters

Parameter	Set values
Size of the melting crucible	1200 cm^3
Furnace temperature	700 °C
Melt temperature	700 °C
The preheating temperature of the mold	200 °C
Runway temperature	750 °C
Stirrer speed	300 rpm
Stirring time	10 min
Applied pressure (for squeeze casting)	100 MPa

a universal testing machine (UTM, Instron 5967) following ASTM standards. The specimen geometry for tensile testing is shown in Figure 5. For testing, three specimens were taken from each fabricated alloy, and the average values of mechanical properties were obtained. The specimens were tested at a 0.001 s^{-1} strain rate at RT (28 °C).

Results and Discussion

Comparative Study of GC and SC AZ91

Figure 6 shows the microstructures of GC and SC AZ91 alloy, analyzed by optical microscopy and FE-SEM. Having α-Mg matrix as the primary phase and secondary β-$Mg_{17}Al_{12}$ precipitates, the distribution of the secondary phase differs in both the alloys. The GC-AZ91 alloy

Table 2. Targeted and Obtained Chemical Composition (wt%) of SC AZ91-Ca-Sr Alloys

Alloy code	Targeted alloy composition	Obtained chemical composition (wt%)						
		Al	Zn	Mn	Si	Ca	Sr	Mg
A1	AZ91	8.9	0.61	0.33	0.019	–	–	Bal.
A2	AZ91-1 wt% Ca–0.3 wt% Sr	8.5	0.50	0.17	0.015	1.04	0.38	Bal.
A3	AZ91-1 wt% Ca–0.6 wt% Sr	8.21	0.49	0.17	0.014	1.12	0.75	Bal.
A4	AZ91-1 wt% Ca–0.9 wt% Sr	8.03	0.47	0.16	0.015	1.09	1.08	Bal.
A5	AZ91-1 wt% Ca–1.2 wt% Sr	7.97	0.46	0.17	0.016	1.13	1.42	Bal.

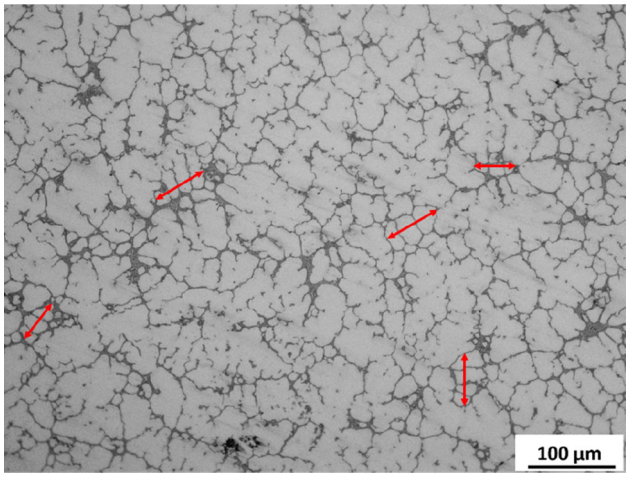

Figure 3. Optical micrograph of A5 alloy and arrows illustrates the measurement of SDAS.

exhibited segregated blocks of β-$Mg_{17}Al_{12}$ precipitates (Figure 6a, c), while the SC-AZ91 micrograph showed the presence of refined and homogeneously distributed β-$Mg_{17}Al_{12}$ precipitates (Figure 6b, d). Such refinement of microstructure has also been previously observed in several studies on squeeze casting of Mg alloys.[12,29,34,35] The faster solidification rate of molten metal in the SC process is the responsible phenomenon for the refinement and scattering of β-$Mg_{17}Al_{12}$ precipitates. The evolution of secondary precipitates is the nonequilibrium solidification process, and hence cooling rate has a significant impact on the distribution and composition of secondary precipitates.[34] In GC, the unavoidable casting defects such as segregation defects or porosity become potential crack initiation sites.[36] The microstructure of GC alloy showed the presence of casting defects such as solidification cracks and blowholes (Figure 4a, c). In comparison, SC produces fine and uniform microstructure with nearly no porosity and casting defects (Figure 4b, d). The obtained results in the present work are in agreement with the earlier reported studies on squeeze cast Mg-Al alloys.[37–39]

The average grain size was calculated using EBSD analysis. The inverse pole figure (IPF) maps, along with the grain size distribution plots for GC and SC AZ91 alloys, are shown in Figure 7. It can be clearly observed that the GC AZ91 IPF map (Figure 7a) consists of larger grains compared to the SC AZ91 map (Figure 7c). The average grain size (AGS) values for both maps were calculated from the grain size distribution graphs in Figure 7b, d.

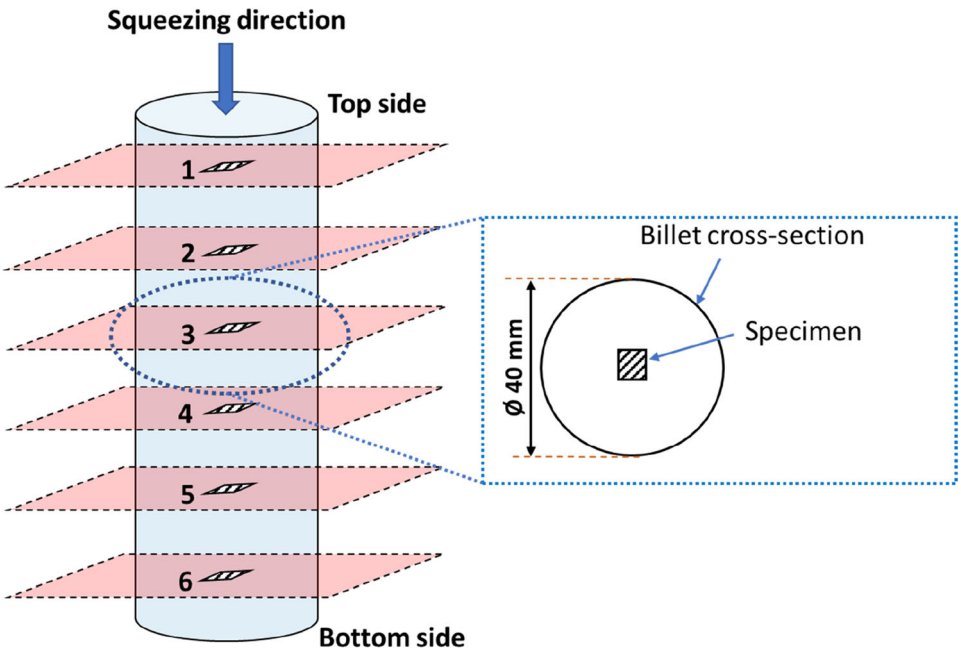

Figure 4. Sample regions for microstructure analysis. (Six samples were extracted from each cylindrical casting).

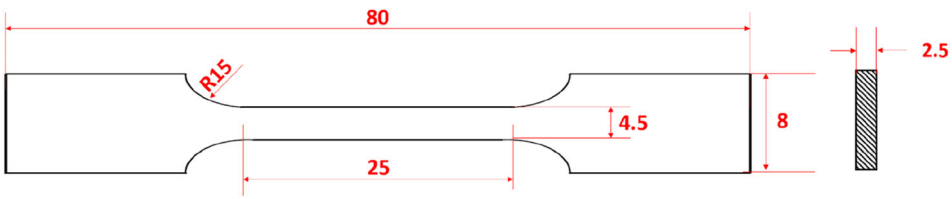

Figure 5. Tensile test specimen (all dimensions are in mm).

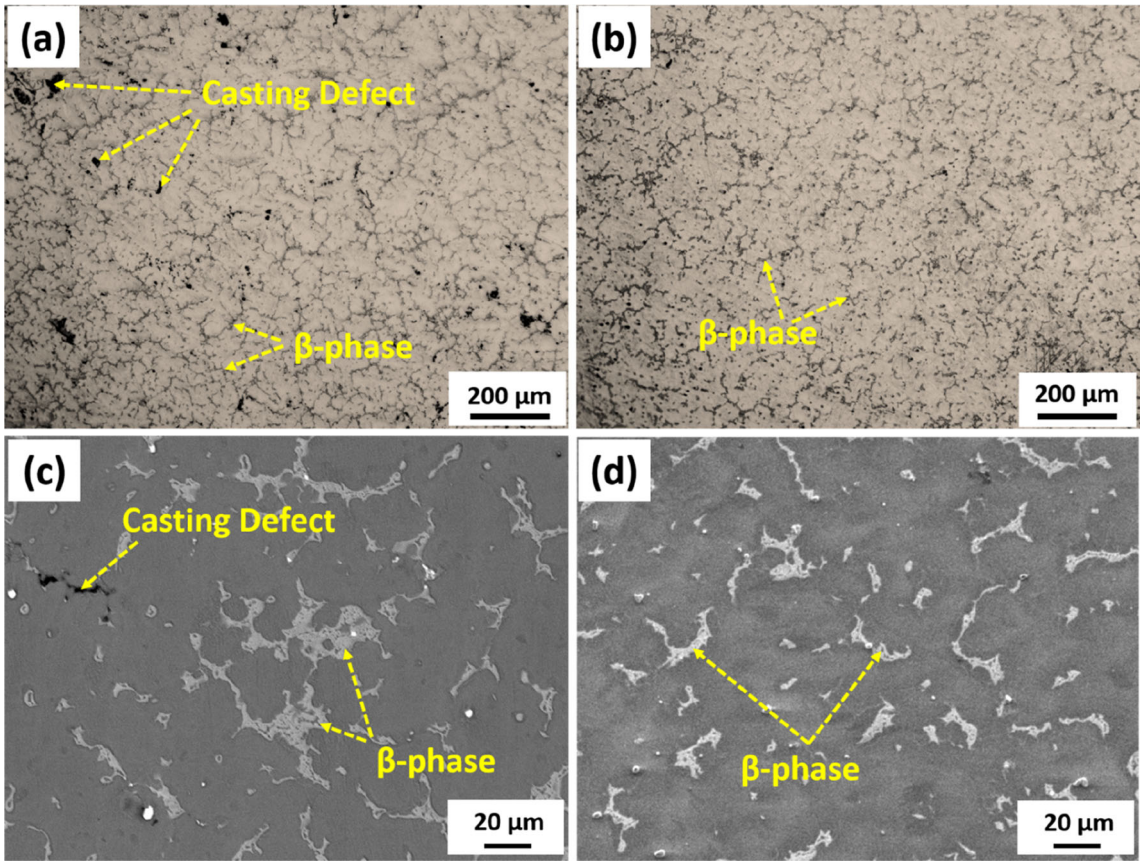

Figure 6. Optical micrograph of (a) GC AZ91, and (b) SC AZ91 Mg alloy, FE-SEM micrographs of (c) GC AZ91 and (d) SC AZ91 Mg alloy.

Figure 7b shows a wide distribution range of grain size (20 µm to 180 µm), with AGS value for GC alloy being 78.58 µm. In contrast, Figure 7d shows a narrower range (18 µm to 140 µm) compared to GC AZ91, with the AGS value of 63.45 µm. The reduction in the distribution of grain size range for SC AZ91 shows the improvement in grain size homogeneity. Table 3 shows the average grain size of the GC and SC AZ91 alloy calculated with six samples from each cylindrical billet. The faster cooling rate in the SC process has a major contribution to grain refinement, and a 20.43% reduction in average grain size was obtained.

Accordingly, the finer microstructure in the SC billet could provide a better condition for subsequent secondary deformation processes for application purposes along with possibly better subsequent mechanical properties.

The cast product generally has a random texture, but practically, during the solidification of metal, the nucleation of grains grows from the surface to the center of the mold due to the temperature gradient between them. This leads to forming casting texture.[40] The second possibility to produce the casting texture is unidirectional squeezing during the solidification of the melt. This phenomenon can be seen in high-pressure die casting methods like squeeze casting.[41] {0001}, {11-20}, and {10-10} pole figures based on EBSD analysis of the GC and SC alloys are shown in Figure 8. In Figure 8a, the pole density points of the pole figures in the GC alloy showed random distribution and the maximum texture intensity is 13.474, whereas the pole figure of SC alloy showed overall random texture but with a strong texture component along squeezing direction at the center of {0 0 0 1} pole figure having maximum intensity at 10.447. The maximum intensity of the texture decreases from 13.474 to 10.447 after squeezing (as shown in Figure 8). In the hexagonal close-packed structure of magnesium, slip occurs mainly on basal planes (0 0 0 1) in <11-20> direction.[33,42] During squeeze casting, the poured material in the mold is subjected to unidirectional pressure before solidification and after solidification. Applied unidirectional pressure in the SC process could be the reason for a texture component along the squeezing direction at the center of {0 0 0 1} pole figure (Figure 8b). The pole figures were generated from the 600 µm × 600 µm area from both GC and SC samples. For equal area, in SC AZ91, grains are finer and higher in numbers compared to the GC AZ91 sample. The higher number of grains in SC AZ91 leads to a decrease in the texture intensity of SC alloy by 22.46%.

The tensile properties of GC and SC AZ91 alloys are shown in Figure 9, which highlights the notable effect of

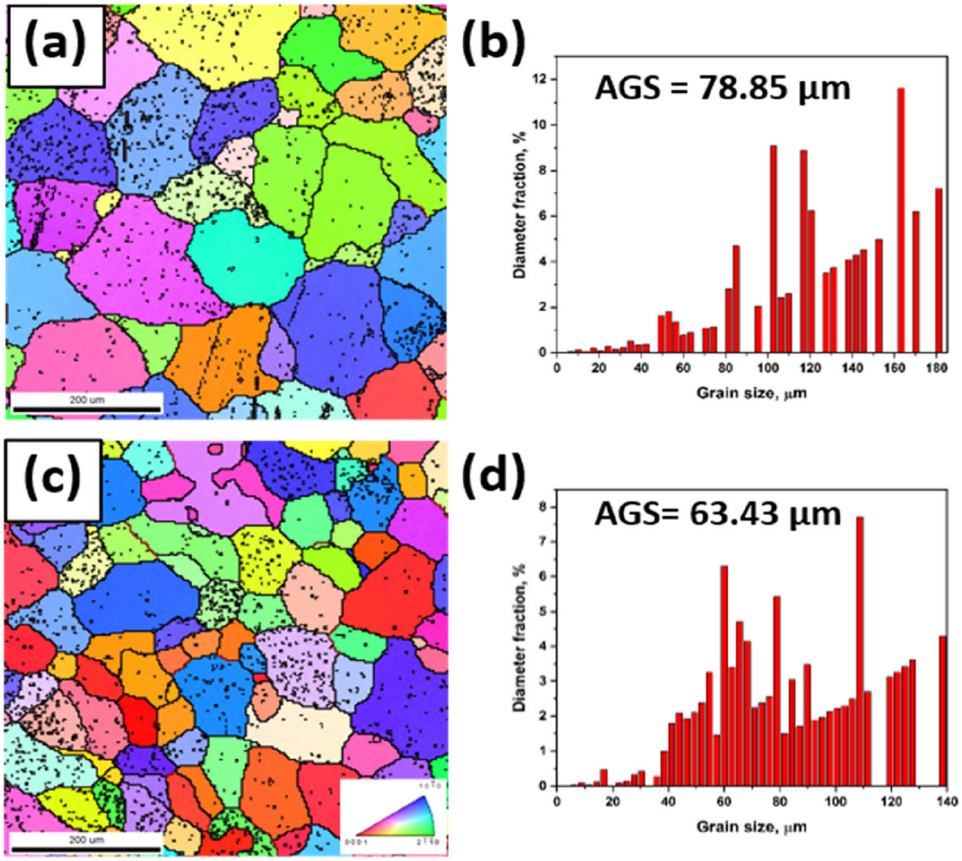

Figure 7. (a) Inverse pole figure (IPF) map of GC AZ91, (b) grain size distribution map of GC AZ91, (c) IPF map of SC AZ91, (d) grain size distribution map of SC AZ91.

Table 3. Measured Average Grain Size (AGS) of GC and SC AZ91 Alloy

Sample	Average grain size (AGS)
GC AZ91	79.2 ± 7.0 µm
SC AZ91	63.02 ± 5.8 µm

castings processes on mechanical properties. All three properties, including tensile yield stress (TYS), ultimate tensile stress (UTS), and % elongation, were improved with the SC process, which can be attributed to quicker solidification and, therefore, finer microstructure. The improvement in mechanical properties in the SC process was found to be 105.3%, 92.6%, and 233.3%, in TYS, UTS, and % elongation, respectively.

There are mainly two reasons behind the improved mechanical properties of SC alloy, namely Hall–Petch strengthening and the reduction in casting defects. With the reduction in grain size (Figure 7), the mechanical properties are observed to be improved.[43] The second reason is the reduction in casting defects in the SC process. As shown in the microstructure analysis by FE-SEM (Figure 6), the GC alloy shows the block β-phase, which is saturated at the grain boundaries and acts as crack nucleation site. Also, the castings defects present in the GC alloys have a detrimental effect on mechanical properties. Hence, the squeeze castings process has proven to be a better method than gravity die casting. Hence, in the present work, the squeeze casting process has been adopted to study the effect of combined alloying additions of Ca and Sr in AZ91 alloy.

Phase Analysis of SC AZ91-Ca-Sr Alloys

The addition of Ca and Sr in magnesium alloy results in the formation of Ca and Sr intermetallics due to their limited solubility in the α-Mg. The XRD measurement data of all SC AZ91-Ca-Sr alloys are shown in Figure 10. The diffraction peaks are well-matched with inorganic crystal structure database (ICSD). From XRD graphs, it is evident that each alloy has primary α-Mg peaks and β-$Mg_{17}Al_{12}$ peaks (ICSD identification number: α-Mg - 654648 and β-$Mg_{17}Al_{12}$ - 158247). Apart from these major phases, SC AZ91-Ca-Sr alloys also show the presence of Al_2Ca and Al_4Sr phases (ICSD identification number: Al_2Ca - 57530 and Al_4Sr - 107887). Ninomiya et al.[44] reported that if the Ca/Al mass ratio were greater than 0.1 in Mg-Al alloy, it resulted in the Al_2Ca intermetallic formation. This was

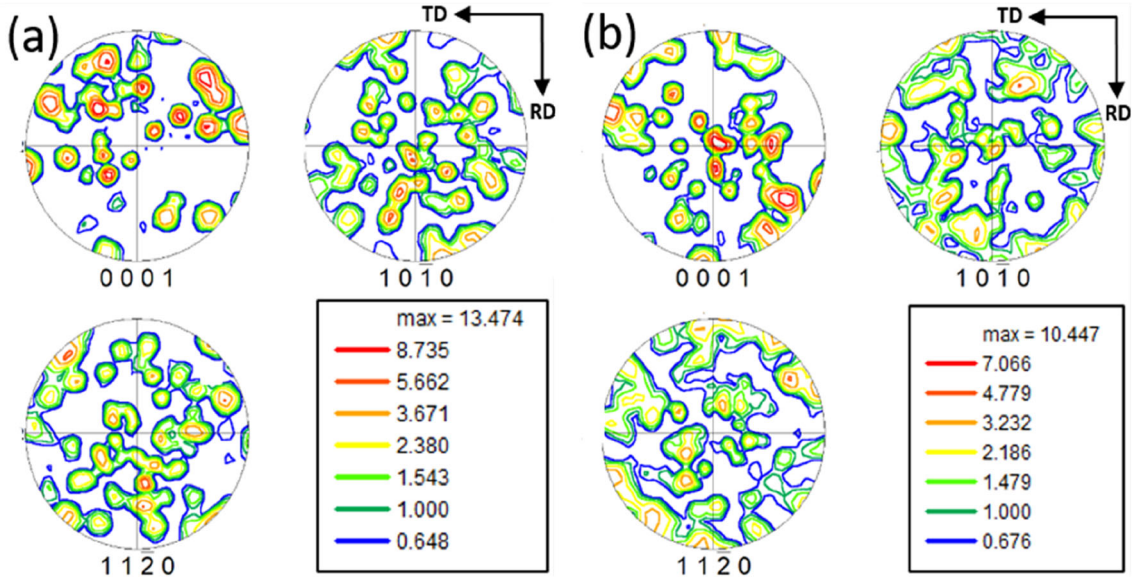

Figure 8. Pole figures of (a) GC AZ91 and (b) SC AZ91 Mg alloy.

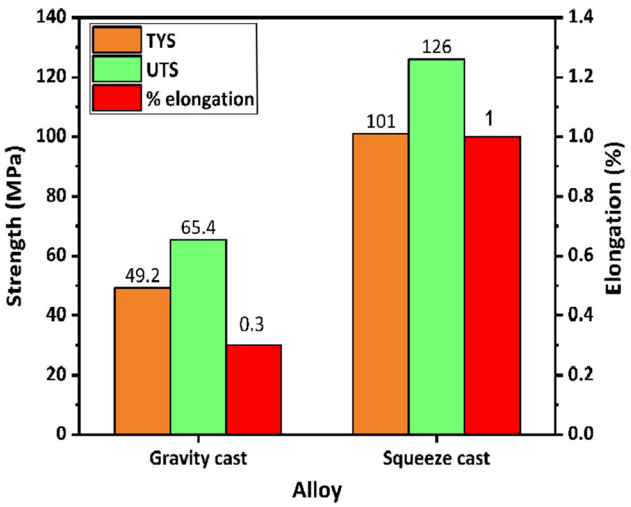

Figure 9. Mechanical properties of GC and SC AZ91 from the tensile test (TYS tensile yield stress, UTS ultimate tensile stress).

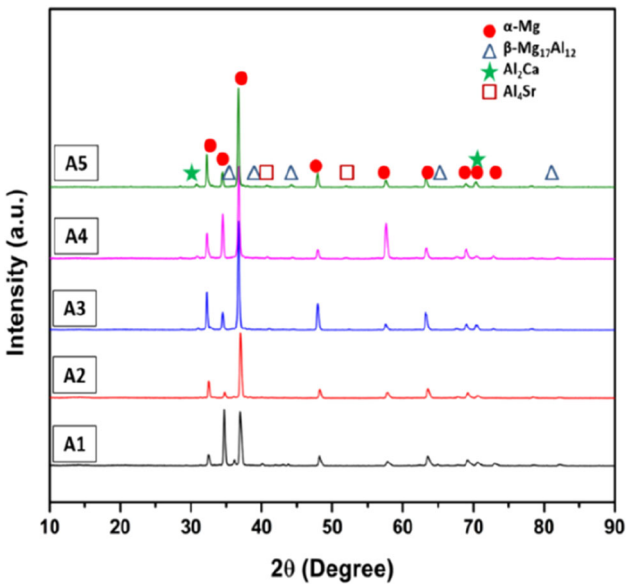

Figure 10. XRD analysis of SC AZ91-Ca-Sr alloys.

consistent with the Mg-Al-Ca ternary phase diagram.[45] Since the values of Ca/Al for all used alloys in the present study were greater than 0.1 (as obtained from the values in Table 2), it can be determined that Al_2Ca is the only Ca-containing phase that can be formed according to the literature.[45] Pekguleryuz et al.[46,47] investigated that the Sr/Al ratios significantly impact phase formation in Mg-Al-Sr ternary alloys. The authors further added that the dominant secondary phases are $Mg_{17}Al_{12}$ and Al_4Sr when the Sr/Al ratio is less than 0.3. The ratio of Sr/Al for all the alloys studied in the present work were less than 0.14. When the Sr/Al ratio is greater than 0.3, a new ternary Mg-Al-Sr compound is formed, which is not found in the present study with XRD analysis. Compared to A1 alloy (base alloy AZ91 as shown in Figure 10), the peak intensity corresponding to the β-$Mg_{17}Al_{12}$ phase decreases with increasing Sr amount (From A1 to A5) while few peaks (at 36.8° and 64.9°) corresponding to β-$Mg_{17}Al_{12}$ phase completely disappear in A5 alloy.

Several works in the literature have discussed β-$Mg_{17}Al_{12}$ suppression with individual Ca and Sr addition.[29,48–51] With the addition of 2 wt% Ca content in cast AZ91, Y. Zhang et al.[29] observed that the formation of the β-$Mg_{17}Al_{12}$ phase is almost suppressed. A similar observation was found by Guohua Wu et al.[48] with 1 wt% Ca addition to the cast AZ91D. With microalloying of Ca, Sr, and Ce (0.2 wt% of each) in the AZ31, L. Shang et al.[49] found the reduction in the amount of β-$Mg_{17}Al_{12}$ phase by forming Al_2Ca, $Al_{11}Ce_3$, Al_2Sr and Al_8CeMn_4 intermetallic phases. The reduction in the volume fraction of β-

$Mg_{17}Al_{12}$ is attributed to very less solubility of Ca and Sr in α-Mg which makes more Ca and Sr available for the formation of second phases such as Al_2Ca and Al_4Sr intermetallics, respectively, at the GBs. Ca features a strong affinity to Al than Mg; hence, Al_2Ca intermetallic is formed, where one unit (in mass) of Ca consumes 1.35 units (in mass) of Al (calculated by the molecular formula[50]). Also, Alireza Sadeghi et al.[51] added the trace level of Sr (0.01 to 0.05 wt%) to cast AZ31 and reported the reduction in volume fraction of β-$Mg_{17}Al_{12}$ by replacing it with the Al_4Sr phase. A similar observation was made by Zhou Ji-Xue et al.[52] with the addition of 0.1 wt% Sr in cast AZ91D. Large atomic radius difference between Sr and Mg results in low maximum equilibrium solid solubility (0.04 at.%).[53] Sr exhibits a strong affinity to Al than Mg and Ca and hence produces the Al_4Sr phase. In AZ91 with combined Ca and Sr addition (alloy A2–A5), Al_2Ca and Al_4Sr phases form earlier than $Mg_{17}Al_{12}$, and it is estimated that they act as nucleation sites for α-Mg.

Microstructural Characterization of SC AZ91-Ca-Sr Alloys

Figure 11 shows the backscattered FE-SEM micrographs of all obtained squeeze cast alloys. Figure 11a shows that the base alloy (A1) contains the α-Mg matrix and semi-continuous β-$Mg_{17}Al_{12}$ phase interdendritic network. The new Al_2Ca and Al_4Sr lamellar phases evolved after the addition of Ca and Sr (Figure 11b–e), which was confirmed by XRD analysis. In the backscattered FE-SEM images, the different phases can be distinguished based on the atomic number of elements present in them. With a higher atomic number of Sr (30) compared to other elements, the Al_4Sr intermetallic looks brighter than Al_2Ca and β-$Mg_{17}Al_{12}$. The Al_2Ca and β-$Mg_{17}Al_{12}$ phases cannot be distinguished from BSE micrographs. Furthermore, the finer and more continuous β-phase network is obtained with increasing Sr addition (Figure 11). The amount of lamellar network is found to enhance with increasing Sr addition which can be attributed to the increasing volume fraction of lamellar Al_4Sr phases. The volume fractions of Al_4Sr phases and the volume fractions of the entire interdendritic network in individual alloy samples are plotted in the form of a graph in Figure 11f, and their values are listed in Table 4. Figure 11 shows that increasing Sr addition results in the increasing volume fraction of the Al_4Sr phase. The increase in the lamellar Al_4Sr network takes place at the expense of a reduction in β-phase since Al has a higher affinity for Sr as discussed earlier. The volume fraction of the interdendritic network has remarkably increased with the increase in Sr amount. As Sr amount increases from 0 wt% (base alloy A1) to 1.2 wt% (A5), the eutectic structure alters from discontinuous to continuous at the GBs. A5 alloy showed the highest volume fraction of the interdendritic network (10.8%) due to the formation of dense secondary phases. Increment in the amount of interdendritic network with Ca and Sr addition has an effect on the secondary dendrite arm spacing (SDAS) of the interdendritic network. The calculated SDAS values for different alloy samples are given in Table 4. Table 4 shows that alloy A5 shows the lowest SDAS. With higher alloy addition, the volume fraction of second phases in the interdendritic network increases. The higher number of nucleating sites leads to an effective reduction in SDAS.[54] In the present work, it can be observed that SDAS started reducing with the increment in Sr addition. The average grain size of the alloy is consistent with the SDAS, with both the values showing decreasing trend with an increase in the interdendritic network with increasing alloy additions. The growth of second phases generally occurs at the surface of grain; hence, an increase in their volume fraction with increasing Sr addition (with Ca amount being constant in all the alloys) reduces the average grain size of alloys and that has been explained later in 'Grain refinement in SC AZ91-Ca-Sr alloys' section.

To study the morphology of individual phases present in the interdendritic network of AZ91-Ca-Sr alloy, the BSE images and their respective EDS point analysis are shown in Figure 12. Figure 12a shows the BSE image of the interdendritic network in A2 alloy (AZ91 -1 wt% Ca–0.3 wt% Sr). Observations based on wt% of elements in spectrums 1, 2 and 3 show $Mg_{17}Al_{12}$, Al_2Ca and Al_4Sr precipitates, respectively. Growing precipitates of Al_2Ca and a few Al_4Sr over the β-$Mg_{17}Al_{12}$ and subsequently replacing bulky β-phase can be observed from the BSE image. Figure 12b shows fully developed lamellar structure of Al_2Ca and Al_4Sr precipitates in the BSE image of the A5 alloy (AZ91 -1 wt% Ca–1.2 wt% Sr). Spectrum 1 shows less bright Al_2Ca structure, whereas spectrums 2 and 3 denote bright Al_4Sr intermetallics. Both Al_2Ca and Al_4Sr form eutectic structures with α-Mg in the interdendritic region.

To ensure the distribution of the Al_4Sr phase, the EDS mapping was carried out for the A2, A3, A4, and A5 samples as shown in Figure 13, which depicts the dispersion of several intermetallics and their corresponding elements. It can be observed that all intermetallics mainly contain Al and also reveal the presence of Ca and Sr in their respective maps, elucidating the evolution of both Al_2Ca and Al_4Sr intermetallics. With Ca content of 1 wt%, most of the Ca dissolved in β-$Mg_{17}Al_{12}$ stimulates the Al_2Ca phase formation and gets distributed at GBs. As expected, the alloy A5 (Figure 13d) with the highest Sr amount of 1.2 % shows maximum Sr-rich regions in the interdendritic network in EDS mapping. Moreover, the matrix regions show very few amounts of Ca and Sr content which indicates that they have significantly less solubility in the matrix (α-Mg) in the case of all four alloys (A2-A5). As all observed intermetallics are Al-based, increasing Al-Ca and Al-Sr amounts suppress the Al-Mg phase formation. The results obtained by EDS analysis are

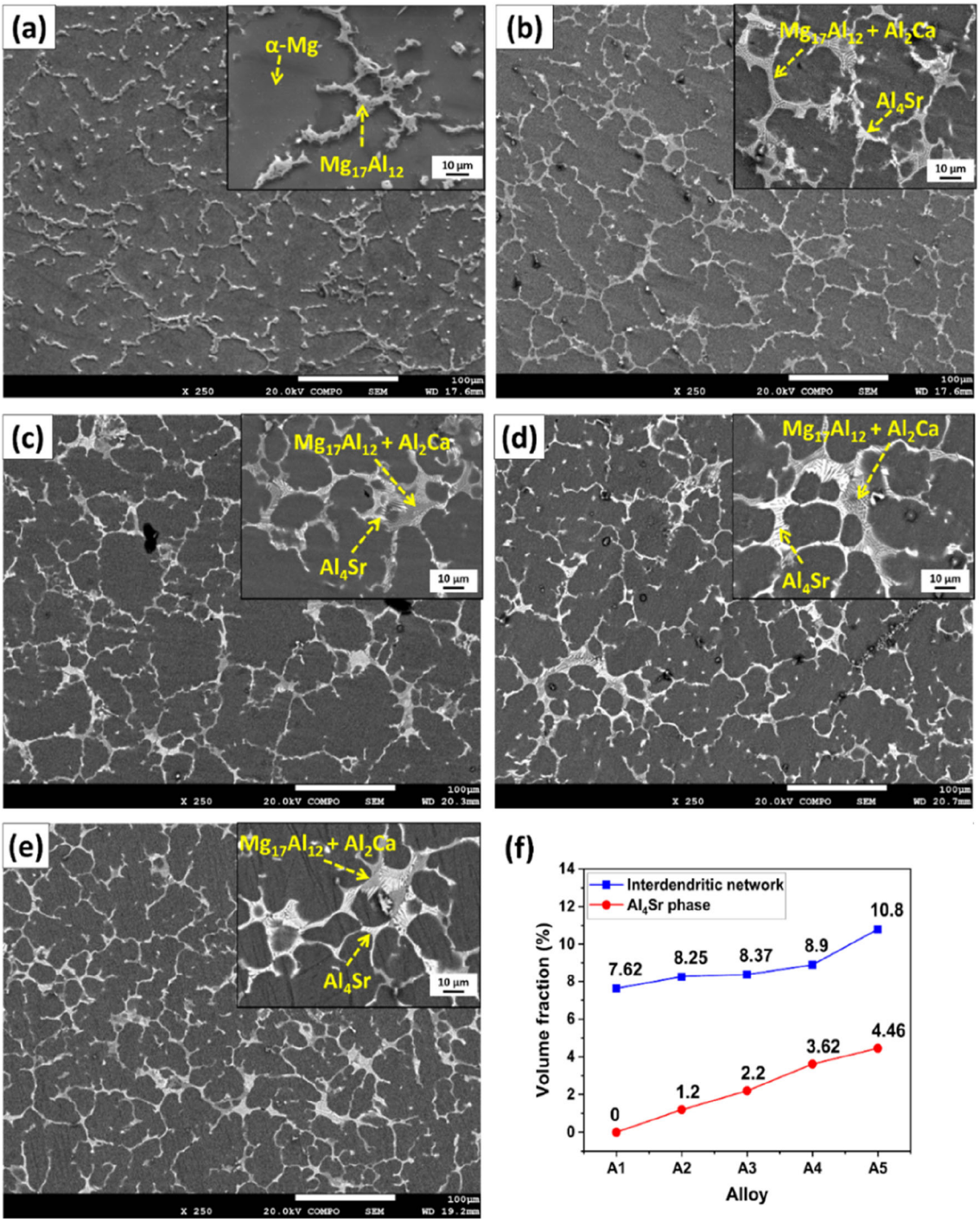

Figure 11. Backscattered electron images of SC AZ91-Ca-Sr alloy with inset image showing the interdendritic network of respective micrographs: (a) A1, (b) A2, (c) A3, (d) A4, (e) A5, (f) volume fraction of interdendritic network and Al_4Sr phase.

consistent with the previously observed FE-SEM results (Figure 11).

In all modified AZ91-Ca-Sr alloys, the secondary eutectic phase refinement can be observed along GBs with Ca+Sr addition, and similar refinement and suppression of β-$Mg_{17}Al_{12}$ have been studied by Chen et al.[55] with Ce (RE metal) additions. The generation of the Al_4Sr intermetallic consumes the Al atoms and reduces the volume of the β-$Mg_{17}Al_{12}$.[56–60] In addition, the Al_4Sr pinned the growth of other phases by acting as a heterogeneous nucleation site.[61,62] Moreover, Sr can show the poisoning effect by getting absorbed in the growing crystal, which could be the reason for the secondary network refinement.[63]

Table 4. Calculated Values of Volume Fraction of Interdendritic Network, Al_4Sr Phase and Secondary Dendrite Arm Spacing (SDAS) of SC AZ91-Ca-Sr Alloys

Alloy	Vol. fraction of interdendritic network (%)	Vol. fraction of Al_4Sr phase (%)	SDAS (μm)
A1	7.62	0	23.66
A2	8.25	1.20	21.05
A3	8.37	2.20	20.35
A4	8.90	3.62	15.10
A5	10.8	4.46	12.53

Grain Refinement in SC AZ91-Ca-Sr Alloys

The grain size of the alloys was calculated by EBSD analysis. From IPF maps obtained using EBSD in Figure 14 for different alloy samples, it can be concluded that the reduction in grain size is obtained from A1 to A2 with the addition of Ca and Sr to AZ91 alloy (Figure 14a, b) and also with subsequent increasing additions of Sr from A2 to A5 (Figure 14b–e). Similar observations were also made in other studies.[50,64,65] Table 5 lists the average grain size (AGS) values for alloy samples A1–A5 and showed gradual reduction in grain size. The gradual reduction in AGS values from A1 to A5 is represented graphically in Figure 14f. The growth restriction factor mechanism (GRF) could explain the Ca+Sr alloying effect on the AGS reduction in the base material. During solidification of AZ91-Ca-Sr alloys, Ca and Sr intermetallics are pinned at the GBs of nucleated grains and restrict their growth. The equation and calculated GRF values are as follows:

$$\mathrm{GRF} = \Sigma_i m_i C_{0,i}(k_i - 1) \qquad \text{Eqn. 1}$$

where m_i is the slope of the liquidus line, k_i is the partition coefficient, $C_{0,i}$ is the initial concentration level, and i is the individual alloying element. For the experimental condition of this work, i denotes Ca and Sr individually. Besides, $m_{Ca} = -12.67$; $m_{Sr} = -3.53$; $k_{Ca} = 0.06$; $k_{Sr} = 0.006$. The $C_{0,Ca}$ and $C_{0,Sr}$ of the AZ91 alloy are given in Table 2.

Therefore, according to Eqn. (1), the calculated GRF values of the A2, A3, A4, and A5 are 13.71, 15.95, 16.75, and 18.42, respectively, showing the grain refinement of SC AZ91-Ca-Sr alloys compared to SC AZ91 without alloying. It is observed that A5 has the highest value of GRF. Therefore, the smallest AGS (49.94 μm) was obtained with 1 wt% Ca + 1.2 wt% Sr addition in alloy A5 (Figure 14) among all the alloys studied in the present work.

Microhardness Analysis

The Vickers microhardness (HV) values of alloy A1–A5 are plotted in Figure 15 and listed in Table 6, showed progressive increase in hardness after alloy additions. The measured average Vicker's hardness value of gravity cast AZ91 alloy is 74 HV. After squeeze casting, AZ91 alloy without addition (A1) shows 87 HV average Vickers hardness (Figure 15). From Figure 15, it can be seen that the hardness value slightly decreases from A1 (87 HV) to A2 (85 HV) with initial Ca and Sr addition to AZ91. Thereafter, hardness is found to increase from A2 (85 HV) to A3 (91 HV) with increasing Sr addition from 0.3% to 0.6%. There is only slight increase (91-92-94 HV) with further Sr additions up to 1.2 % (A3-A5). The increasing amount of harder Al_4Sr particles from A2 to A5 alloy samples reduces the penetration depth of the indenter under load thus providing higher values of microhardness. Moreover, reduction in grain size is another factor in the improvement of hardness with increasing Sr addition. The fine grain size produces a high grain boundary density in the microstructure which could act as a resistance to the indentation. Alloy A5 showed the lowest grain size (47 μm) and correspondingly highest hardness value (94 HV) among all the alloys studied in the present work. The improvement of hardness with reduction in grain size has also been discussed in previous studies in the literature.[66–69]

Tensile Properties

The values of TYS, UTS and % elongation studied using tensile tests for all the alloy samples in the present study are given in Table 6. The variation in various tensile properties with change of composition for A1–A5 samples is also plotted in Figure 16. It can be observed that the TYS and UTS values decrease from A1 to A2 alloy by 13.86% and 18.25%, respectively. A2 alloy displays the initial transition of β-phase morphology from coarse to skeleton-like structure. Also, the volume fraction of β-$Mg_{17}Al_{12}$ decreases in A2 alloy due to the alloying additions of Ca and Sr. The decrease in strength values from A1 to A2 and the corresponding increase in elongation are estimated to be due to the decreasing volume fraction of β-$Mg_{17}Al_{12}$ which is the major strengthening phase in AZ91 alloy. Further additions of Sr of 0.6% and 0.9% (A3 and A4) alloys result in the continuous improvement of both TYS and UTS. The TYS and UTS values improved from A2 to A3 by 20.62% and 30.09% and from A3 to A4 by 4.76% and 18.65%, respectively. The improvement in strength is attributed to the increasing amount of Sr and a corresponding reduction in SDAS and grain size (as listed in Table 6). Furthermore, Ca and Sr additions result in the formation of the skeletal structure of secondary phases in which β-$Mg_{17}Al_{12}$ network is also refined. All these favorable factors bring about an increase in the tensile properties from A2 to A4 alloy. Generally, it has been reported in previous studies that with increasing Sr amount in AZ91, needle-shaped Sr-containing phases emerge at the grain boundaries. These phases boost material strength by preventing dislocation movement, but they may also act as

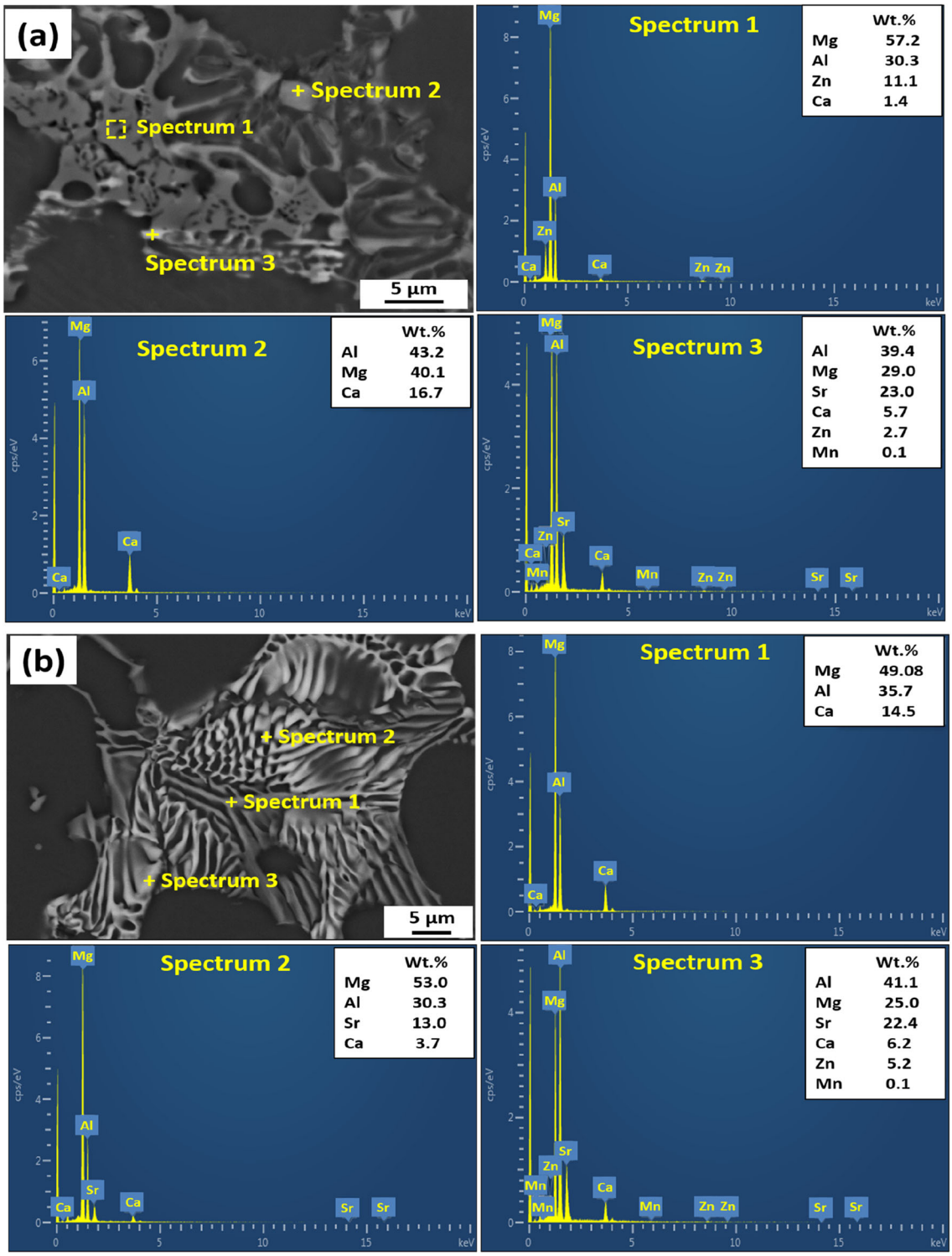

Figure 12. Backscattered electron images of (a) A2 alloy (AZ91-1 wt% Ca–0.3 wt% Sr) and (b) A5 alloy (AZ91-1 wt% Ca–1.2 wt% Sr) with EDS spectrum of marked points in their respective BSE image.

a stress raiser during loading.[56] In contrast, the Sr addition with Ca in the current work develops the skeleton-like structure of Al_4Sr and decreases the possibility of crack initiation compared to the needle-shaped structure. The tensile properties are observed to degrade with further addition of 1.2% Sr (A5). It can be seen that the TYS and UTS values for A5 samples are the lowest among all the samples, along with a decrease in percentage elongation value. In spite of A5 alloy having the lowest grain size (49.94 µm) and SDAS (12.53 µm), the inferior tensile

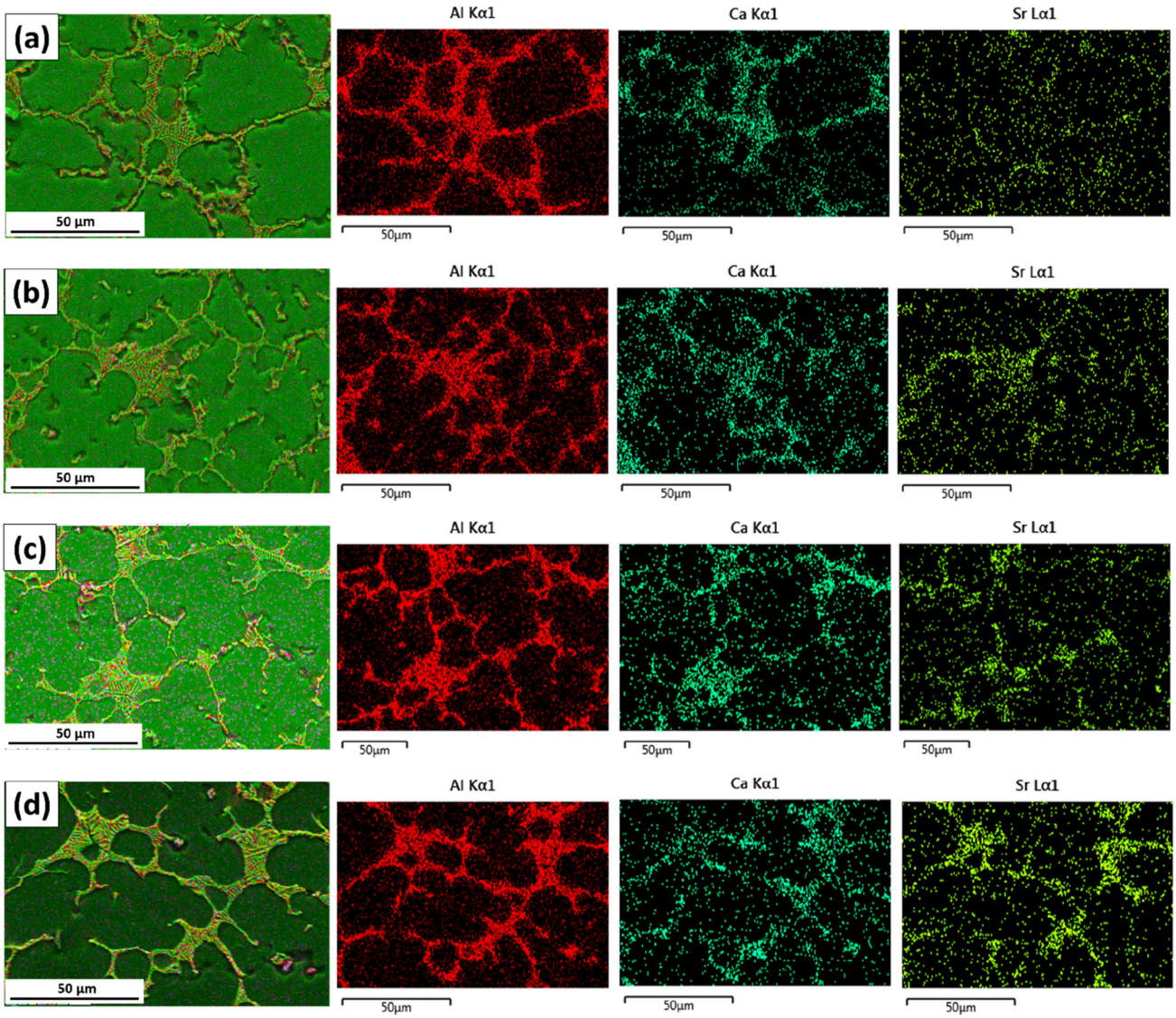

Figure 13. EDS map taken for alloy (a) A2, (b) A3, (c) A4, (d) A5.

properties are the result of the coarsening of secondary phases and the amount of interdendritic network reaching the saturation level thereby inducing brittleness in the microstructure. The best combination of tensile properties was obtained for alloy sample A4 containing 0.9% Sr. The combined addition of Ca and Sr (Ca+Sr) increases to 2.2% from 1.9% from A4 to A5 alloy samples. Previously, in the study by Yang Zhang et al.[29] it was found that more than 2 wt% of Ca addition in AZ91D induced brittleness in the material and hence deteriorated UTS and % elongation, whereas in another work by Fan et al.[31] the addition of 2 wt% Sr in AZ91D alloy led to a decrease in TYS was observed. It should be noted that the strength values decreased from A1 to A2, while percentage elongation increased. There was a reduction in grain size as well as SDAS from A1 to A2; however, this did not lead to an increase in the strength values. Therefore, it can be concluded that the decreasing volume fraction of β-$Mg_{17}Al_{12}$ and embrittling effect of Ca-containing phases were more dominant than other factors. In general, homogenization heat treatment techniques could significantly improve the mechanical properties of AZ91 (with or without alloy additions) owing to dissolution of β-phase and providing solid solution strengthening effect in the material.[54,57]

Conclusion

In the present work, the effect of squeeze casting was studied in AZ91 Mg alloy by comparison with gravity die-cast AZ91 alloy. Further, an investigation on the effect of combined additions of Ca and Sr to AZ91 alloy was performed by the study of microstructure and mechanical properties of squeeze cast AZ91-Ca-Sr alloys. The major conclusions from the work are listed below:

1. Squeeze casting (SC) of AZ91 alloy produced a high-quality billet with more refined grains and

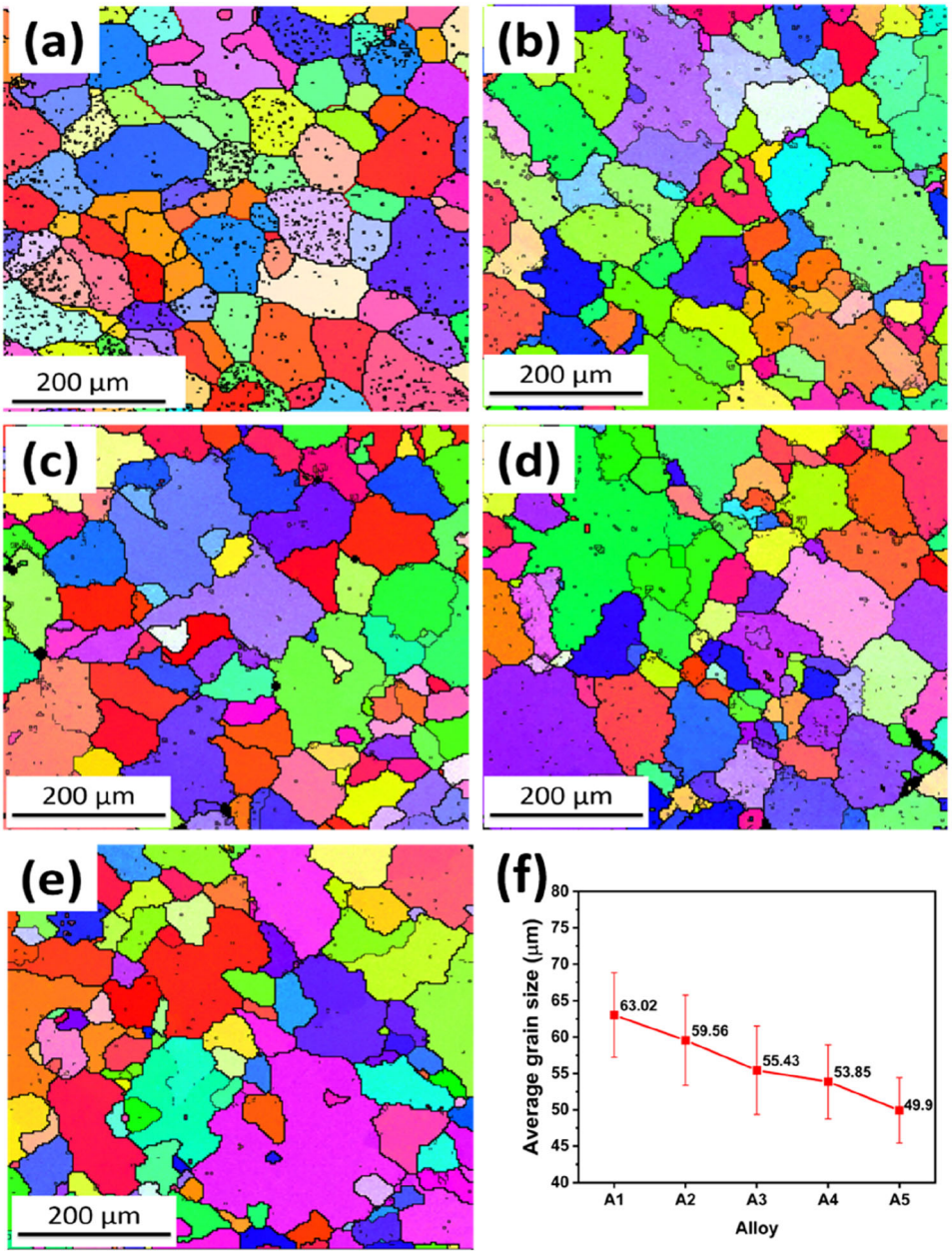

Figure 14. IPF maps of squeeze cast alloys (a) A1, (b) A2, (c) A3, (d) A4, (e) A5, and (f) average grain size map.

Table 5. Calculated Values of Average Grain Size (AGS) from IPF Map of SC AZ91-Ca-Sr Alloys

Alloy	Average grain size, AGS (µm)
A1	63.02 ± 5.8
A2	59.56 ± 6.2
A3	55.43 ± 6.1
A4	53.85 ± 5.1
A5	49.94 ± 4.5

uniform microstructure with improved mechanical properties than gravity die-cast (GC) AZ91 alloy. The improvement in mechanical properties from GC to SC alloys was found to be 105.3%, 92.6%, and 233.3%, in YS, UTS, and % elongation, respectively. Finer microstructure in the SC billet could provide a better condition for subsequent secondary deformation processes for application purposes.

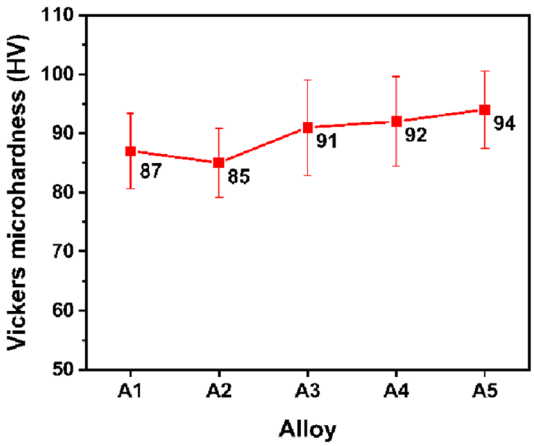

Figure 15. Vickers microhardness for squeeze cast AZ91-Ca-Sr alloy.

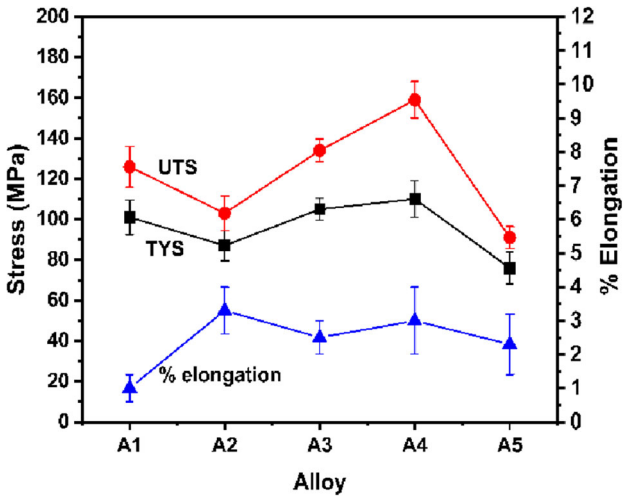

Figure 16. Tensile properties of squeeze cast AZ91-Ca-Sr alloys in tensile testing at RT* TYS *tensile yield stress,* UTS *ultimate tensile stress.

2. Applied unidirectional pressure in the mold during the SC process generated a texture component along the squeezing direction at the center of {0 0 0 1} pole figure although a slight decrement in the maximum texture intensity has been found with the SC process due to the smaller grain size compared to GC AZ91 Mg alloy.
3. With the Ca and Sr addition to the SC AZ91 alloy, a continuous and finer interdendritic network was obtained, and the formation of lamellar Al_2Ca and Al_4Sr phases was observed with the suppression of the β-$Mg_{17}Al_{12}$ phase.
4. With the highest GRF value (18.42) and reduced SDAS (12.53 μm), SC AZ91-1 wt% Ca–1.2 wt% Sr (A5) alloy showed the smallest average grain size (AGS-49.94 μm) among all the alloys in the present study.
5. Microhardness was found to decrease slightly from A1 (base alloy)–A2 (AZ91-1 wt% Ca–0.3 wt% Sr) alloy. Thereafter, an increase in Sr level from 0.3 wt% to 1.2 wt% in SC AZ91 alloy resulted in an increase in microhardness values. The highest improvement in microhardness has been found in SC A5 (AZ91-1 wt% Ca–1.2 wt% Sr) alloy by 8.04% compared with the base SC AZ91 alloy.
6. The mechanical properties of SC AZ91-Ca-Sr alloys were found to be affected by grain size, volume fraction of intermetallics and SDAS. With initial Ca + Sr addition to SC AZ91 in A2 alloy, the TYS and UTS were found to be decreased due to embrittling effect of Ca-containing phases. Further additions of Sr from 0.3 wt% to 0.9 wt% (A2–A5) improved the TYS and UTS. The alloy SC A4 (AZ91-1 wt% Ca–0.9 wt% Sr) showed the optimum combination of mechanical properties (i.e., TYS, UTS and % elongation), whereas more than 1.9 wt% Ca+Sr addition deteriorates mechanical properties by inducing brittleness in the microstructure due to saturation of Ca- and Sr-containing second phases.

Table 6. Calculated Values of Volume Fraction of Interdendritic Network and Al_4Sr Phase, Secondary Dendrite Arm Spacing (SDAS), Average Grain Size (AGS), Hardness, and Tensile Properties of SC AZ91-Ca-Sr Alloys

Alloy	Vol. fraction of interdendritic network (%)	Vol. fraction of Al_4Sr phase (%)	SDAS (μm)	AGS (μm)	Hardness (HV)	Tensile properties		
						TYS (MPa)	UTS (MPa)	% El
A1	7.62	0	23.66	63.02 ± 5.8	87 ± 6.4	101 ± 8.6	126 ± 10.1	1.0 ± 0.4
A2	8.25	1.20	21.05	59.56 ± 6.2	85 ± 5.8	87 ± 7.5	103 ± 8.5	3.3 ± 0.7
A3	8.37	2.20	20.35	55.43 ± 6.1	91 ± 8.1	105 ± 5.4	134 ± 5.6	2.5 ± 0.5
A4	8.90	3.62	15.10	53.85 ± 5.1	92 ± 7.6	110 ± 9.0	159 ± 8.9	3.0 ± 1.0
A5	10.8	4.46	12.53	49.94 ± 4.5	94 ± 6.6	76 ± 7.8	91 ± 5.5	2.3 ± 0.9

Acknowledgements

The author Ankush S. Marodkar would like to thank the Ministry of Education, Government of India, for providing teaching assistantship for doctoral studies. The authors express their gratitude to the sophisticated instrumentation centre (SIC), IIT Indore, for providing the facilities for research work.

Conflict of interest On behalf of all the authors, the corresponding author states that there is no conflict of interest.

REFERENCES

1. A. Bankoti, A. Mondal, S. Kumar, B. Ray, Individual and combined additions of calcium and antimony on microstructure and mechanical properties of squeeze-cast AZ91D magnesium alloy. Mater. Sci. Eng. A **626**, 186–194 (2015). https://doi.org/10.1016/j.msea.2014.12.068
2. H. Borkar, M. Hoseini, M. Pekguleryuz, Effect of strontium on the texture and mechanical properties of extruded Mg–1% Mn alloys. Mater. Sci. Eng. A **549**, 168–175 (2012). https://doi.org/10.1016/j.msea.2012.04.029
3. L. Wang, R. Lett, S. Felicelli, J. Berry, J. Jordon, D. Penrod, Microstructure and performance of four casting processes for magnesium alloy AZ91. Int. J. Met. **5**, 37–46 (2011). https://doi.org/10.1007/BF03355521
4. Y. Zhao, Z. Pu, L. Wang, D. Liu, Modeling of grain refinement and nucleation behavior of Mg-4Y-0.5Zr (wt.%) alloy via cellular Automaton model. Int. J. Met. **16**, 945–961 (2022). https://doi.org/10.1007/s40962-021-00654-z
5. B. Mordike, T. Ebert, Magnesium: properties-applications-potential. Mater. Sci. Eng. A **302**(1), 37–45 (2001). https://doi.org/10.1016/S0921-5093(00)01351-4
6. A. Luo, M. Pekguleryuz, Cast magnesium alloys for elevated temperature applications. J. Mater. Sci. **29**, 5259–5271 (1994). https://doi.org/10.1007/BF01171534
7. L. Urtekin, H.B. Özerkan, C. Cogun, A. Genc, Z. Esen, F. Bozkurt, Experimental investigation on wire electric discharge machining of biodegradable AZ91 Mg alloy. J. Mater. Eng. Perform. **30**(10), 7752–7761 (2021). https://doi.org/10.1007/s11665-021-05939-2
8. F. Czerwinski, Controlling the ignition and flammability of magnesium for aerospace applications. Corros. Sci. **86**, 1–16 (2014). https://doi.org/10.1016/j.corsci.2014.04.047
9. S.J. Huang, S. Diwan Midyeen, M. Subramani, C.C. Chiang, Microstructure evaluation, quantitative phase analysis, strengthening mechanism and influence of hybrid reinforcements (β-sicp, bi and sb) on the collective mechanical properties of the AZ91 magnesium matrix. Metals **11**, 898 (2021). https://doi.org/10.3390/met11060898
10. E. Tolouie, R. Jamaati, Effect of β–$Mg_{17}Al_{12}$ phase on microstructure, texture and mechanical properties of AZ91 alloy processed by asymmetric hot rolling. Mater. Sci. Eng. A **738**, 81–89 (2018). https://doi.org/10.1016/j.msea.2018.09.086
11. L. Zhang, Q. Wang, W. Liao, W. Guo, B. Ye, H. Jiang, W. Ding, Effect of homogenization on the microstructure and mechanical properties of the repetitive-upsetting processed AZ91D alloy. J. Mater. Sci. Technol. **33**, 935–940 (2017). https://doi.org/10.1016/j.jmst.2017.01.015
12. Y. Cubides, A.I. Karayan, M. Vaughan, I. Karaman, H. Castaneda, Enhanced mechanical properties and corrosion resistance of a fine-grained Mg-9Al-1Zn alloy: the role of bimodal grain structure and β-$Mg_{17}Al_{12}$ precipitates. Mater. **13**, 100840 (2020). https://doi.org/10.1016/j.mtla.2020.100840
13. A. Bankoti, A. Mondal, C.S. Perugu, B. Ray, S. Kumar, Correlation of microstructure and electrochemical corrosion behavior of squeeze-cast Ca and Sb added AZ91 Mg alloys. Metall. Mater. Trans. A **48**, 5106–5121 (2017). https://doi.org/10.1007/s11661-017-4244-1
14. M. Khosroaghayani, M. Khorasanian, S.R. Alavi Zaree, M. Eskandari, Investigation of microstructure and mechanical properties of AZ91 magnesium alloy produced by directional solidification method in different angles using cafe simulation. Int. J. Met. (2022). https://doi.org/10.1007/s40962-022-00766-0
15. A. Elsayed, C. Ravindran, B.S. Murty, Effect of aluminum-titanium-boron based grain refiners on AZ91E magnesium alloy grain size and microstructure. Int. J. Met. **5**, 29–41 (2011). https://doi.org/10.1007/BF03355470
16. S. Saha, C. Ravindran, Grain refinement of AZ91E and Mg-9 wt.% Al binary alloys using zinc oxide. Int. J. Met. **9**, 33–42 (2015). https://doi.org/10.1007/BF03355600
17. A. Azad, L. Bichler, A. Elsayed, Effect of a novel Al-SiC grain refiner on the microstructure and properties of AZ91E magnesium alloy. Int. J. Met. **7**, 49–59 (2013). https://doi.org/10.1007/BF03355564
18. A. Koltygin, V. Bazhenov, U. Mahmadiyorov, Influence of Al–5Ti–1B master alloy addition on the grain size of AZ91 alloy. J. Magnes. Alloy. **5**, 313–319 (2017). https://doi.org/10.1016/j.jma.2017.08.002
19. Y. Lu, Q. Wang, X. Zeng, W. Ding, C. Zhai, Y. Zhu, Effects of rare earths on the microstructure, properties and fracture behavior of Mg–Al alloys. Mater. Sci. Eng. A **278**, 66–76 (2000). https://doi.org/10.1016/S0921-5093(99)00604-8
20. W. Qudong, L. Yizhen, Z. Xiaoqin, D. Wenjiang, Z. Yanping, L. Qinghua, L. Jie, Study on the fluidity of AZ91+ xRE magnesium alloy. Mater. Sci. Eng. A

271, 109–115 (1999). https://doi.org/10.1016/S0921-5093(99)00185-9
21. P. Cui, M. Hu, Z. Ji, X. Hongyu, L. Naizhi, Y. Zhehua, Effect of La/Nd ratio on the microstructure and corrosion behaviors of squeeze-cast Mg–Al–Zn–La–Nd alloys. Int. J. Met. (2022). https://doi.org/10.1007/s40962-022-00767-z
22. E. Baril, P. Labelle, M. Pekguleryuz, Elevated temperature Mg-Al-Sr: creep resistance, mechanical properties, and microstructure. JOM **55**, 34–39 (2003). https://doi.org/10.1007/s11837-003-0207-7
23. B. Jing, S. Yangshan, X. Shan, X. Feng, Z. Tianbai, Microstructure and tensile creep behavior of Mg–4Al based magnesium alloys with alkaline-earth elements Sr and Ca additions. Mater. Sci. Eng. A **419**, 181–188 (2006). https://doi.org/10.1016/j.msea.2005.12.017
24. J. Yan, Y. Sun, F. Xue, J. Bai, S. Xue, W. Tao, Creep deformation mechanism of magnesium-based alloys. J. Mater. Sci. **43**, 6952–6959 (2008). https://doi.org/10.1007/s10853-008-2968-4
25. I. Gokalp, A. Incesu, Effect of Ca addition to the elevated temperature mechanical properties of AZ series magnesium alloys. Int. J. Met. (2022). https://doi.org/10.1007/s40962-022-00872-z
26. I.A. Anyanwu, Y. Gokan, S. Nozawa, A. Suzuki, S. Kamado, Y. Kojima, S. Takeda, T. Ishida, Development of new die-castable Mg-Zn-Al-Ca-RE alloys for high temperature applications. Mater. Trans. **44**, 562–570 (2003). https://doi.org/10.2320/matertrans.44.562
27. I.A. Anyanwu, Y. Gokan, A. Suzuki, S. Kamado, Y. Kojima, S. Takeda, T. Ishida, Effect of substituting cerium-rich mischmetal with lanthanum on high temperature properties of die-cast Mg–Zn–Al–Ca–RE alloys. Mater. Sci. Eng. A **380**, 93–99 (2004). https://doi.org/10.1016/j.msea.2004.03.039
28. X. Feng, M. Xuegang, S. Yangshan, Microstructures and mechanical properties of AZ91 alloy with combined additions of Ca and Si. J. Mater. Sci. **41**, 4725–4731 (2006). https://doi.org/10.1007/s10853-006-0060-5
29. Y. Zhang, G. Wu, W. Liu, L. Zhang, S. Pang, Y. Wang, W. Ding, Effects of processing parameters and Ca content on microstructure and mechanical properties of squeeze casting AZ91–Ca alloys. Mater. Sci. Eng. A **595**, 109–117 (2014). https://doi.org/10.1016/j.msea.2013.12.014
30. M. O. Pekguleryuz, E. Baril, Magnesium Technology, J.N. Hryn ed., 2001, pp. 283–289
31. Y. Fan, G. H. Wu, C. Q. Zhai, Effect of strontium on mechanical properties and corrosion resistance of AZ91D. Mater. Sci. Forum (Trans. Tech. Publ.), 546–549, 67-570 (2007). https://doi.org/10.4028/www.scientific.net/MSF.546-549.567
32. P. Zhao, Q. Wang, C. Zhai, Y. Zhu, Effects of strontium and titanium on the microstructure, tensile properties and creep behavior of AM50 alloys. Mater. Sci. Eng. A **444**, 318–326 (2007). https://doi.org/10.1016/j.msea.2006.08.111
33. H. Borkar, M. Hoseini, M. Pekguleryuz, Effect of strontium on flow behavior and texture evolution during the hot deformation of Mg–1 wt% Mn alloy. Mater. Sci. Eng. A **537**, 49–57 (2012). https://doi.org/10.1016/j.msea.2012.01.029
34. J. Bai, Y. Sun, F. Xue, J. Qiang, Microstructures and creep properties of Mg–4Al–(1–4) La alloys produced by different casting techniques. Mater. Sci. Eng. A **552**, 472–480 (2012). https://doi.org/10.1016/j.msea.2012.05.072
35. H. Yu, S. Chen, W. Yang, Y. Zhang, S. Chen, Effects of rare element and pressure on the microstructure and mechanical property of AZ91D alloy. J. Alloys Compd. **589**, 479–484 (2014). https://doi.org/10.1016/j.jallcom.2013.12.019
36. M. Horynová, J. Zapletal, P. Doležal, P. Gejdoš, Evaluation of fatigue life of AZ31 magnesium alloy fabricated by squeeze casting. Mater. Des. **45**, 253–264 (2013). https://doi.org/10.1016/j.matdes.2012.08.079
37. T.M. Yue, H. Ha, N. Musson, Grain size effects on the mechanical properties of some squeeze cast light alloys. J. Mater. Sci. **30**, 2277–2283 (1995). https://doi.org/10.1007/BF01184573
38. M. Masoumi, H. Hu, Influence of applied pressure on microstructure and tensile properties of squeeze cast magnesium Mg–Al–Ca alloy. Mater. Sci. Eng. A **528**, 3589–3593 (2011). https://doi.org/10.1016/j.msea.2011.01.032
39. S. Kleiner, O. Beffort, A. Wahlen, P. Uggowitzer, Microstructure and mechanical properties of squeeze cast and semi-solid cast Mg–Al alloys. J. Light Met. **2**, 277–280 (2002). https://doi.org/10.1016/S1471-5317(03)00012-9
40. T. Le, Q. Wei, J. Wang, P. Jin, M. Chen, J. Ma, Effect of different casting techniques on the microstructure and mechanical properties of AE44-2 magnesium alloy. Mater. Res. Express **7**, 116513 (2020). https://doi.org/10.1088/2053-1591/abc721
41. J. Sheng, L. Wang, Y. Zhao, S. Xu, X. Liu, W. Fei, Effect of solution treatment on the texture and tensile properties of Mg2B2O5W/2024Al composite. J. Alloys Compd. **701**, 716–721 (2017). https://doi.org/10.1016/j.jallcom.2017.01.080
42. H. Borkar, M. Pekguleryuz, Microstructure and texture evolution in Mg–1 %Mn–Sr alloys during extrusion. J. Mater. Sci. **48**, 1436–1447 (2013). https://doi.org/10.1007/s10853-012-6896-y
43. G.E. Dieter, *Mechanical Metallurgy, SI*, metric. (McGraw-Hill Book Co., London, 1988)
44. R. Ninomiya, T. Ojiro, K. Kubota, Improved heat resistance of Mg-Al alloys by the Ca addition. Acta Metall. Mater. **43**(2), 669–674 (1995). https://doi.org/10.1016/0956-7151(94)00269-N

45. J. Catterall, R. Pleasance, The constitution of magnesium-rich magnesium-aluminum-calcium alloys. J. Inst. Metals **86** (1957)
46. M.O. Pekguleryuz, A.A. Kaya, Creep resistant magnesium alloys for powertrain applications. Adv. Eng. Mater. **5**, 866–878 (2003). https://doi.org/10.1002/adem.200300403
47. M. Parvez, M. Medraj, E. Essadiqi, A. Muntasar, G. Denes, Experimental study of the ternary magnesium–aluminium–strontium system. J. Alloys Compd. **402**, 170–185 (2005). https://doi.org/10.1016/j.jallcom.2005.04.173
48. G. Wu, Y. Fan, H. Gao, C. Zhai, Y.P. Zhu, The effect of Ca and rare earth elements on the microstructure, mechanical properties and corrosion behavior of AZ91D. Mater. Sci. Eng. A **408**, 255–263 (2005). https://doi.org/10.1016/j.msea.2005.08.011
49. L. Shang, S. Yue, R. Verma, P. Krajewski, C. Galvani, E. Essadiqi, Effect of microalloying (Ca, Sr, and Ce) on elevated temperature tensile behavior of AZ31 magnesium sheet alloy. Mater. Sci. Eng. A **528**(10–11), 3761–3770 (2011). https://doi.org/10.1016/j.msea.2011.01.094
50. W. Qudong, C. Wenzhou, Z. Xiaoqin, L. Yizhen, D. Wenjiang, Z. Yanping, X. Xiaoping, Effects of Ca addition on the microstructure and mechanical properties of AZ91magnesium alloy. J. Mater. Sci. **36**, 3035–3040 (2001). https://doi.org/10.1023/A:1017927109291
51. A. Sadeghi, M. Pekguleryuz, Microstructure, mechanical properties and texture evolution of AZ31 alloy containing trace levels of strontium. Mater. Charact. **62**, 742–750 (2011). https://doi.org/10.1016/j.matchar.2011.05.006
52. J.-X. Zhou, W. Jie, W. Jing, Y.-S. Yang, Effects of RE and Sr additions on dendrite growth and phase precipitation in AZ91D magnesium alloy. Trans. Nonferrous Met. Soc. China **20**, s331–s335 (2010). https://doi.org/10.1016/S1003-6326(10)60492-X
53. F. Hehmann, F. Sommer, B. Predel, Extension of solid solubility in magnesium by rapid solidification. Mater. Sci. Eng. A **125**, 249–265 (1990). https://doi.org/10.1016/0921-5093(90)90175-3
54. C.H. Caceres, C. Davidson, J. Griffiths, C. Newton, Effects of solidification rate and ageing on the microstructure and mechanical properties of AZ91 alloy. Mater. Sci. Eng. A **325**, 344–355 (2002). https://doi.org/10.1016/S0921-5093(01)01467-8
55. W. Chen, J. Kong, W. Chen, Effect of rare earth Ce on the microstructure, physical properties and thermal stability of a new lead-free solder. J. Min. Metall. B Metall. **47**, 11–21 (2011). https://doi.org/10.2298/JMMB1101011C
56. H.L. Zhao, S. Guan, F. Zheng, Effects of Sr and B addition on microstructure and mechanical properties of AZ91 magnesium alloy. J. Mater. Res. **22**, 2423–2428 (2007). https://doi.org/10.1557/jmr.2007.0331
57. A. Afsharnaderi, M. Lotfpour, H. Mirzadeh, M. Emamy, M. Malekan, Enhanced mechanical properties of as-cast AZ91 magnesium alloy by combined RE-Sr addition and hot extrusion. Mater. Sci. Eng. A **792**, 139817 (2020). https://doi.org/10.1016/j.msea.2020.139817
58. Y.A. Chen, J. Gao, Y. Song, Y. Wang, The influences of Sr on the microstructure and mechanical properties of Mg-5Zn-2Al alloy. Mater. Sci. Eng. A **671**, 127–134 (2016). https://doi.org/10.1016/j.msea.2016.06.033
59. H. Xi, C. Jihua, Y. Hongge, S. Bin, Z. Guanghao, M. Chongming, Effects of minor Sr addition on microstructure and mechanical properties of the as-cast Mg–4.5 Zn–4.5 Sn–2Al-based alloy system. J. Alloys Compd. **579**, 39-44 (2013). https://doi.org/10.1016/j.jallcom.2013.05.036
60. Z. Zareian, M. Emamy, M. Malekan, H. Mirzadeh, W. Kim, A. Bahmani, Tailoring the mechanical properties of Mg–Zn magnesium alloy by calcium addition and hot extrusion process. Mater. Sci. Eng. A **774**, 138929 (2020). https://doi.org/10.1016/j.msea.2020.138929
61. L. Chen, M. Liang, G. Zhao, J. Zhou, C. Zhang, Microstructure evolution of AZ91 alloy during hot extrusion process with various ram velocity. Vaccuum **150**, 136–143 (2018). https://doi.org/10.1016/j.vacuum.2018.01.036
62. J. Zhang, Z. Leng, M. Zhang, J. Meng, R. Wu, Effect of Ce on microstructure, mechanical properties and corrosion behavior of high-pressure die-cast Mg–4Al-based alloy. J. Alloys Compd. **509**(3), 1069–1078 (2011). https://doi.org/10.1016/j.jallcom.2010.09.185
63. Q. Qin, Y. Zhao, W. Zhou, P. Cong, Effect of phosphorus on microstructure and growth manner of primary Mg2Si crystal in Mg2Si/Al composite. Mater. Sci. Eng. A **447**(1–2), 186–191 (2007). https://doi.org/10.1016/j.msea.2006.10.076
64. D. Zhang, D. Zhang, F. Bu, X. Li, K. Guan, Q. Yang, S. Liu, X. Liu, J. Meng, Effects of minor Sr addition on the microstructure, mechanical properties and creep behavior of high pressure die casting AZ91-0.5 RE based alloy, Mater. Sci. Eng. A **693**, 51–59 (2017). https://doi.org/10.1016/j.msea.2017.03.055
65. K. Hirai, H. Somekawa, Y. Takigawa, K. Higashi, Effects of Ca and Sr addition on mechanical properties of a cast AZ91 magnesium alloy at room and elevated temperature. Mater. Sci. Eng. A **403**, 276–280 (2005). https://doi.org/10.1016/j.msea.2005.05.028
66. H. Zengin, Y. Turen, L.A. Elen, Comparative study on microstructure, mechanical and tribological properties of A4, AE41, AS41 and AJ41 magnesium alloys. J. Mater. Eng. Perform. **28**, 4647–4657 (2019). https://doi.org/10.1007/s11665-019-04223-8
67. C. Yim, K. Shin, Changes in microstructure and hardness of rheocast AZ91HP magnesium alloy with

stirring conditions. Mater. Sci. Eng. A **395**, 226–232 (2005). https://doi.org/10.1016/j.msea.2004.12.050
68. G. M. Lule Senoz, T. A. Yilmaz, Optimization of Equal Channel Angular Pressing Parameters for Improving the Hardness and Microstructure Properties of Al–Zn–Mg Alloy by Using Taguchi Method. Met. Mater. Int. **27**, 436–448 (2021). https://doi.org/10.1007/s12540-020-00730-9
69. Y. Xu, F. Gensch, Z. Ren, K.U. Kainer, N. Hort, Effects of Gd solutes on hardness and yield strength of Mg alloys. Prog. Nat. Sci. Mater. Int. **28**, 724–730 (2018). https://doi.org/10.1016/j.pnsc.2018.10.002